Earth and Planetary Science Letters 416 (2015) 82–90

Contents lists available at ScienceDirect

Earth and Planetary Science Letters

www.elsevier.com/locate/epsl

A rock-mechanical assessment of Mercury's global tectonic fabric

Christian Klimczak [a,b,*], Paul K. Byrne [b,c], Sean C. Solomon [b,d]

[a] Department of Geology, University of Georgia, Athens, GA 30602, USA
[b] Department of Terrestrial Magnetism, Carnegie Institution of Washington, Washington, DC 20015, USA
[c] Lunar and Planetary Institute, Houston, TX 77058, USA
[d] Lamont-Doherty Earth Observatory, Columbia University, Palisades, NY 10964, USA

ARTICLE INFO

Article history:
Received 21 July 2014
Received in revised form 12 November 2014
Accepted 5 February 2015
Available online xxxx
Editor: C. Sotin

Keywords:
near-surface rock strength
rock failure
planetary tectonics
faulting
global contraction
Mercury

ABSTRACT

Mercury's global tectonic history is thought to have been dominated by two major processes: tidal despinning and global contraction. Each process is expected to have produced a distinctive global stress field and resultant fault pattern. Thousands of thrust-fault-related landforms documented on Mercury can be attributed to global contraction, but no global signature of tidal despinning has been conclusively documented. Because global contraction operated throughout an extended portion of Mercury's geologic history, any tidal despinning pattern either would have formed together with global contraction, or would have been modified by global contraction after despinning was complete. Here, we reassess global fracture patterns predicted to result from tidal despinning and from a combination of tidal despinning and global contraction. We specifically make use of rock strength and deformability parameters appropriate for Mercury's fractured lithosphere. Results indicate that a tidal despinning pattern would consist only of a global set of opening-mode fractures (joints) in the upper part of the lithosphere, whereas the combination of tidal despinning and global contraction would have produced a global population of thrust faults, with no preferred orientations in the polar regions but with an increasing preference for north–south orientations toward the equator. If an equatorial bulge from an early state of rapid spin was supported by Mercury's lithosphere, two end-member scenarios for the timing and duration of these two processes may be considered. In one, tidal despinning predated global contraction; in the other, tidal despinning and global contraction overlapped in time. We test the predictions of both scenarios against the distribution and orientations of Mercury's tectonic landforms. The global pattern of thrust faults is generally consistent with predictions for the scenario under which tidal despinning and global contraction temporally overlapped.

1. Introduction

Since the Mariner 10 spacecraft returned the first images of tectonic landforms on Mercury (Strom et al., 1975), the prospect that a global tectonic fabric is preserved on the planet has been discussed in light of two major processes – tidal despinning (Burns, 1976; Melosh, 1977; Melosh and Dzurisin, 1978; Melosh and McKinnon, 1988) and global contraction (Watters and Nimmo, 2010; Watters et al., 1998, 2009) – or some combination of the two (Pechmann and Melosh, 1979; Dombard and Hauck, 2008; Matsuyama and Nimmo, 2009; Beuthe, 2010). The absolute and relative magnitudes of stresses resulting from the relaxation of an equatorial tidal bulge that would have accompanied a decrease in Mercury's spin rate were predicted to have been sufficiently large to pervasively fracture the planet's lithosphere, producing a distinctive "despinning" pattern (Melosh and McKinnon, 1988). This pattern includes an equatorial province of north–south-orientated thrust faults, a zone of northeast–southwest- and northwest–southeast-trending strike-slip faults in the middle latitudes, and a region of east–west-orientated normal faulting in the polar regions (Fig. 1). In contrast, near-surface stresses resulting from global contraction due to secular cooling of Mercury's interior (Solomon, 1977) were predicted to be horizontally isotropic (Melosh and McKinnon, 1988), yielding a global tectonic pattern of contractional structures generally devoid of any preferred orientations (Melosh and McKinnon, 1988) even if locally influenced by topographic stresses or pre-existing zones of weakness. Finally, combinations of stresses from global contraction and tidal despinning were predicted to produce a global population of thrust faults with preferred north–south (Pechmann and Melosh, 1979; Dombard and Hauck, 2008) or east–west (Beuthe, 2010) orientations.

* Corresponding author at: Department of Geology, University of Georgia, Athens, GA 30602, USA.
E-mail address: klimczak@uga.edu (C. Klimczak).

http://dx.doi.org/10.1016/j.epsl.2015.02.003
0012-821X/

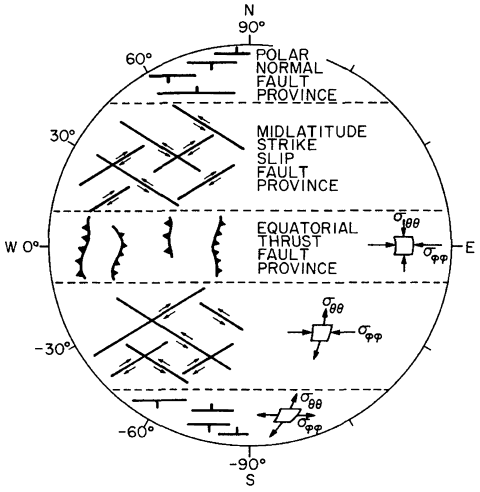

Fig. 1. The global fracture pattern for Mercury predicted to result from tidal despinning, after Melosh (1977). Despinning is thought to produce a global tectonic fabric with a thrust fault province at the equator consisting of mainly north–south structures, northeast–southwest- and northwest–southeast-oriented strike-slip faults in the mid-latitudes, and a normal fault province with east–west-oriented structures at each pole.

The validity of these proposed global tectonic patterns can be questioned, however, on the grounds that no previous studies evaluated relative stress magnitudes with respect to the deformability of a fractured lithosphere in the assessment of modes of fracturing and corresponding fracture orientations. Further, possible differences in the timing and duration of tidal despinning and global contraction were not discussed previously with respect to the fracturing mechanisms that would ensue.

After more than three years of orbital operations, the MErcury Surface, Space ENvironment, GEochemistry, and Ranging (MESSENGER) mission has acquired data showing that the innermost planet has preserved abundant tectonic landforms, of which thrust faults (Fig. 2) are the largest and most widely distributed type of structure (Byrne et al., 2014). The global contraction of Mercury accommodated by mapped thrust faults alone is equivalent to a cumulative decrease in planetary radius of as much as 7 km (Byrne et al., 2014), far more than previously estimated (Watters et al., 1998, 2009; Watters and Nimmo, 2010; Di Achille et al., 2012). Regional tectonic patterns include fold and thrust belts in excess of 1000 km in length (Byrne et al., 2014), thrust faults that follow the rims of large basins for hundreds of kilometers (Fassett et al., 2012; Byrne et al., 2014), and thrust faults that border expanses of high-standing terrain (Byrne et al., 2014). Moreover, mapping and kinematic analyses suggest the presence of strike-slip motions along some of the major scarps (Massironi et al., 2015; Galluzzi et al., 2015). Nonetheless, a global tectonic fabric similar to those suggested to have resulted from tidal despinning (e.g., Fig. 1) is not readily evident.

In this paper, we investigate stress magnitudes and latitudinal stress variations originating from tidal despinning, as well as from the combination of tidal despinning and global contraction, following the framework summarized by Melosh and McKinnon (1988). In contrast to previous work, however, we assess these problems by considering the elastic properties of the lithosphere with the aid of engineering rock mass classifications (Bieniawski, 1989), which include conditions for rock failure, fracture mechanisms, and fracture orientations evaluated for a basaltic rock mass (Schultz, 1995). We then compare these findings to MESSENGER observations, and we appraise our results with respect to the possible timing and duration of despinning and global contraction on Mercury.

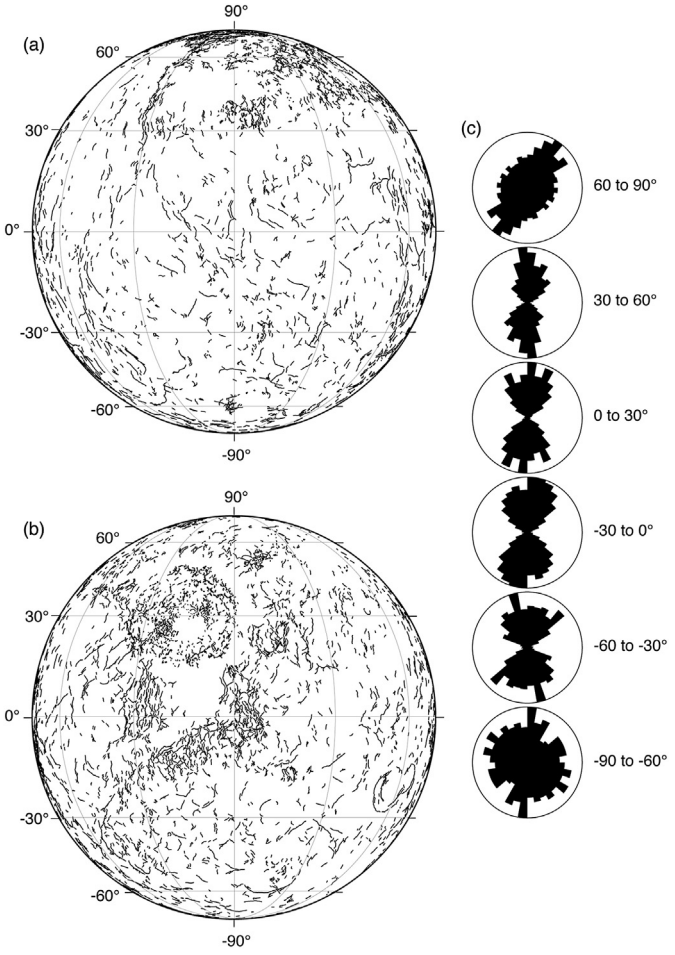

Fig. 2. Global distribution of thrust-fault-related landforms on Mercury (Byrne et al., 2014). (a) Orthographic view of Mercury centered at 0°N, 0°E. (b) Orthographic view of Mercury centered at 0°N, 180°E. Graticules are shown in 30° increments. (c) Rose diagrams in 30° latitudinal bins from north (top) to south (bottom), indicating orientations of the major thrust faults. Thrust faults have preferred north–south orientations between 60°N and 60°S but do not show a preferred orientation at the poles.

2. Tidal despinning, global contraction, and the deformability of planetary lithospheres

2.1. Stresses from tidal despinning and global contraction

Mercury is locked in a 3:2 spin–orbit resonance: It rotates three times about its spin axis for every two orbits about the Sun, with a sidereal rotational period of approximately 59 Earth days. However, it is assumed that Mercury's initial rotational period may have been as short as 20 h, as its spin angular momentum would then compare well with those of most other planets (Kaula, 1968; Burns, 1975). The required change in spin rate would have been accompanied by the relaxation of an equatorial bulge (Burns, 1976; Melosh, 1977; Melosh and McKinnon, 1988), with an accompanying change in near-surface principal stresses in a thin elastic lithosphere (Vening-Meinesz, 1947) given in spherical coordinates by:

$$\sigma_{\theta\theta} = -\frac{5}{24}\Delta m \frac{E}{5+\nu}(5 - 3\cos 2\lambda) \tag{1a}$$

and

$$\sigma_{\phi\phi} = \frac{5}{24}\Delta m \frac{E}{5+\nu}(1 + 9\cos 2\lambda), \tag{1b}$$

where the term Δm is the difference between the initial and final ratios of the centripetal acceleration at the equator to the gravitational acceleration, E is Young's modulus, ν is Poisson's ratio, and λ is the latitude at which the stresses are evaluated. The stresses $\sigma_{\theta\theta}$ and $\sigma_{\phi\phi}$ are defined as the meridional (north–south) and azimuthal (east–west) horizontal stress components, respectively, and are positive in compression.

The near-surface horizontal stresses for global contraction of a planet of radius R associated with a change in planetary radius ΔR may be estimated in their simplest forms (Melosh and McKinnon, 1988) from the expressions:

$$\sigma_{\theta\theta} = \sigma_{\phi\phi} = \frac{E}{1-\nu}\frac{\Delta R}{R}. \quad (2)$$

With this relation, a 1-km radius change on Mercury corresponds to stresses on the order of 100 MPa, a value believed to be adequate to produce large-scale thrust faulting on the planet (Melosh and McKinnon, 1988; Watters and Nimmo, 2010).

2.2. Deformability of planetary lithospheres

Young's modulus in Eqs. (1) and (2) is strictly appropriate only for an intact rock sample (Walsh, 1965; Kulhawy, 1975; Segall, 1984; Kachanov, 1992; Schultz, 1996). However, tidal despinning and planetary contraction operate globally – a scale at which Mercury's lithosphere is not likely ever to have been intact. Instead, its lithosphere very probably has been characterized throughout its geological history by a combination of intact rock and associated structural weaknesses, such as fractures, impact damage zones, and lithologic contacts, which together tend to weaken the overall material. Data returned by the Gravity Recovery and Interior Laboratory (GRAIL) spacecraft (e.g., Zuber et al., 2013) show that, for the Moon, impact-generated fracturing introduced a substantial porosity to the upper crust that may even extend to depths of tens of kilometers (Wieczorek et al., 2013).

The rock mass rating (RMR) system, measured on a scale from 0 to 100, where 100 represents intact rock, can account for the degree and condition of weaknesses (as well as for pore pressure conditions) within a rock (Bieniawski, 1989) to evaluate better its strength parameters on larger scales (Schultz, 1993, 1995, 1996). The concept of RMR has previously been applied to planetary settings to assess the strength properties of basaltic rock masses on Venus (Schultz, 1993) and of sedimentary rock masses on Mars (Nahm and Schultz, 2007), as well as to general fault-scaling relations on the terrestrial planets (Schultz et al., 2006).

Measured surface elemental abundances on Mercury are consistent with compositions well matched by low-iron, magnesian basalts (Nittler et al., 2011; Weider et al., 2012), so near-surface stresses from tidal despinning and global contraction should be assessed with the strength and deformational properties for Mercury's lithosphere appropriate to those of a basaltic rock mass. Basaltic rock masses usually have RMR values between 45 and 75 (Bieniawski, 1989; Schultz, 1993, 1995, 1996). Although it is very likely that the uppermost portion of Mercury's lithosphere is affected by an even higher degree of fracturing, comparable to that indicated for the Moon by the findings from the GRAIL mission (e.g., Wieczorek et al., 2013), we use these RMR values as conservative upper and lower bounds for estimates of the in situ modulus of deformation (or deformation modulus), E^*, which replaces Young's modulus in Eqs. (1) and (2). Empirical studies have shown that E^* is relatively insensitive to rock type, and that it relates to RMR as

$$E^* = 2\mathrm{RMR} - 100 \quad \text{for RMR} > 50 \quad (3a)$$

and

$$E^* = 10^{(\mathrm{RMR}-10)/40} \quad \text{for RMR} < 50, \quad (3b)$$

with units of E^* given in GPa (see Bieniawski, 1989). Deformation moduli for RMR values of 75 are about $E^* \approx 50$ GPa, whereas an RMR of 45 yields a deformation modulus $E^* \approx 7.5$ GPa. Compared with traditionally used values for Young's modulus of $E \approx 160$ GPa (Melosh, 1977) or $E = 100$ GPa (Dombard and Hauck, 2008), the calculated deformation moduli in this study are substantially lower.

2.3. Reassessment of magnitudes and latitudinal variations of global stresses

Solutions for the stress field from tidal despinning, as given by Eq. (1) but adjusted for the deformation moduli for RMR values of 45 and 75, are shown in Fig. 3. Stresses from tidal despinning alone are shown in Fig. 3a. An initial spin period of 20 h has been assumed (e.g., Kaula, 1968; Burns, 1975). The stresses depend on the deformation modulus, with stress magnitudes for an RMR value of 45 substantially lower than those for an RMR value of 75. As described by Melosh (1977), the azimuthal and meridional stress components are equal at the poles, but elsewhere the azimuthal component is always greater, defining three global provinces in which the principal stresses have the same relative magnitudes. In province 1a, which spans the region between latitudes 90° and 48.5°, all horizontal stress components are tensile (i.e., $\sigma_{\theta\theta} \leq \sigma_{\phi\phi} < 0$). At latitudes 48.5°N and 48.5°S (province 2a), the azimuthal stress component is zero and the meridional stress component is tensile (i.e., $\sigma_{\theta\theta} < \sigma_{\phi\phi} = 0$). In province 3a, the region between 48.5°N and 48.5°S, meridional stresses are still tensile, but azimuthal stresses are compressive (i.e., $\sigma_{\theta\theta} < 0 < \sigma_{\phi\phi}$).

Another set of stresses is explored for a combination of tidal despinning and global contraction (Fig. 3b). As shortening structures are observed globally (Fig. 2), we assume that Mercury's entire lithosphere is under compression. If stresses from global contraction (Eq. (2)) are superposed on the global stress field resulting from tidal despinning (Dombard and Hauck, 2008), a value of ΔR of at least 2.9 km must be assumed to achieve a globally compressive stress field.

Differential stresses (i.e., $\sigma_1 - \sigma_3$) for this scenario remain unchanged (Fig. 3b) compared with the case of tidal despinning alone (Fig. 3a). However, the stress magnitudes change, so that if ΔR is precisely 2.9 km then the polar regions are in a tectonically neutral regime, in which neither tensile nor compressive stresses prevail (i.e., $\sigma_{\theta\theta} \leq \sigma_{\phi\phi} \sim 0$). Stresses become increasingly compressive toward the equator, and the azimuthal component becomes increasingly greater than the meridional component ($0 < \sigma_{\theta\theta} < \sigma_{\phi\phi}$).

These results show that stresses from tidal despinning and/or global contraction, although consistent with previous studies in their latitudinal variations (e.g., Melosh, 1977; Dombard and Hauck, 2008), are substantially lower in magnitude than those obtained in studies in which the properties of intact rock were assumed. The lower stresses calculated here warrant further evaluation as to whether rock failure is predicted. For that assessment, we evaluate basaltic rock mass strengths with respect to the predicted stress conditions caused by the two tidal despinning scenarios in Fig. 3 (i.e., despinning alone, and despinning plus global contraction just sufficient for a globally compressive stress field).

3. Strength of a basaltic rock mass

The brittle strength of a rock may be assessed with the empirical Hoek–Brown failure criterion (Hoek and Brown, 1980), given

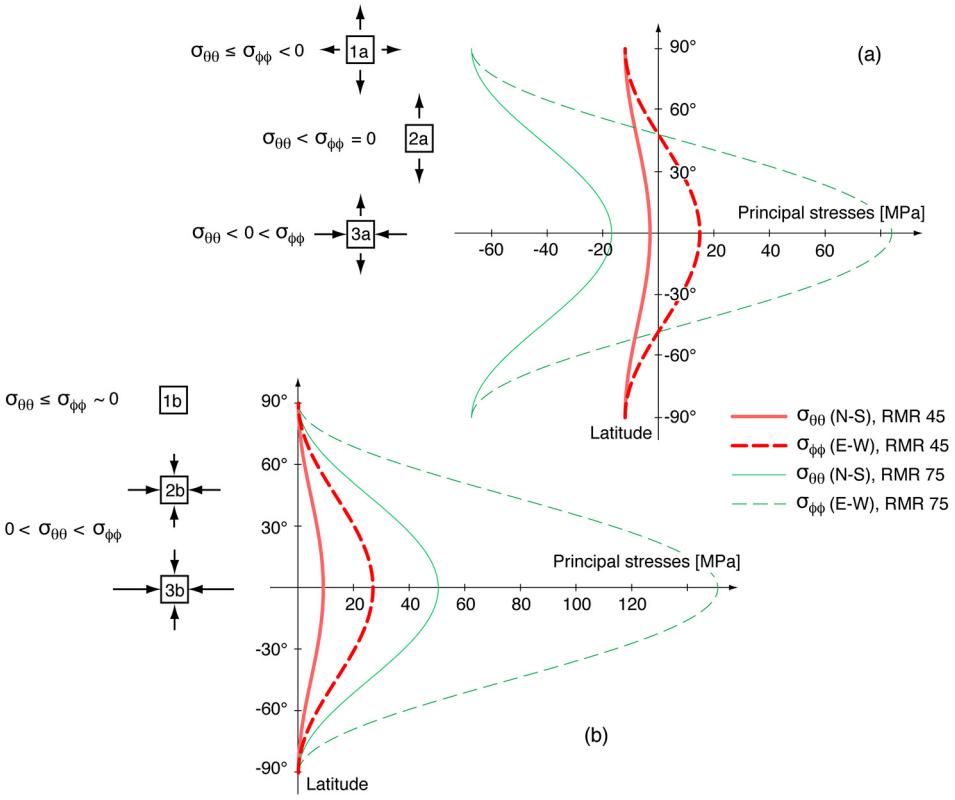

Fig. 3. Variation with latitude of the meridional (solid lines) and azimuthal (dashed lines) stress components, for rock mass rating (RMR) values of 45 (thick red lines) and 75 (thin green lines), resulting from tidal despinning from an original spin period of 20 h and the relaxation of the equivalent equatorial bulge. Compression is shown as positive. Note that stress magnitudes obtained for RMR values of 45 are substantially smaller than those calculated for RMR values of 75. (a) Stress distributions from tidal despinning alone result in purely tensile stresses in the polar regions, and compressive azimuthal but tensile meridional stresses between latitudes 48.5°N and 48.5°S. (b) Stress distributions from tidal despinning superposed on stresses from global contraction. A globally compressional stress state is attained as long as the decrease in Mercury's radius is 2.9 km (as shown) or greater.

by:

$$\sigma_1 = \sigma_3 + \sqrt{m\sigma_c\sigma_3 + s\sigma_c^2}, \tag{4}$$

where σ_1 and σ_3 are the greatest and least principal stresses and σ_c is the uniaxial (or unconfined) compressive strength. The variables m and s are rock-specific parameters, for which Bieniawski (1989, p. 178) defined relationships for a correlation with RMR, whereby

$$m = m_i \exp\left(\frac{\mathrm{RMR} - 100}{28}\right) \tag{5a}$$

and

$$s = \exp\left(\frac{\mathrm{RMR} - 100}{9}\right). \tag{5b}$$

The parameter m_i represents the initial value of m for intact rock. Values for m_i depend on the rock type, and a detailed list was provided by Bieniawski (1989, p. 179ff). Strength parameters for a range of RMR values of basaltic rock masses were given by Schultz (1993). In that same study, Schultz (1993) also determined that the minimum depth to which a basaltic rock mass of RMR = 45 on Mercury controls strength must be ~4.5 km, providing a reference depth value above (i.e., shallower than) which the Hoek–Brown criterion tied to RMR is well suited for the assessment of brittle failure in Mercury's lithosphere.

The strength of a rock mass can be rewritten in the form of a Mohr envelope (Schultz, 1993) as:

$$\sigma_n = \sigma_3 + \frac{\tau_{\max}^2}{\tau_{\max} + \frac{m\sigma_c}{8}} \tag{6a}$$

and

$$\tau = (\sigma_n - \sigma_3)\sqrt{1 + \frac{m\sigma_c}{4\tau_{\max}}}, \tag{6b}$$

where σ_n represents the normal stress and τ the shear stress, with $\tau_{\max} = (\sigma_1 - \sigma_3)/2$. Mohr envelopes for intact basalts and for basaltic rock masses with RMR values of 75 and 45 are depicted in Fig. 4. Where normal and shear stresses fall inside the envelope (i.e., below the curve), stable conditions are predicted, whereas where stresses fall outside the envelope (i.e., above the curve), rock failure is predicted. Furthermore, tensile stresses that predict failure facilitate the formation of mode-I fractures (joints, dikes), whereas purely compressive stresses facilitate mode-II + III fractures (normal faults, thrust faults) (Schultz, 1996). As noted earlier, intact basalts are substantially stronger than basaltic rock masses with RMR values of 75 and 45.

The strength envelopes (Fig. 4) can be used to assess whether stresses resulting from tidal despinning (Eq. (1); Fig. 3a), or from a combination of tidal despinning and global contraction (Eqs. (1) and (2); Fig. 3b), are sufficient to initiate fracturing. If failure is predicted, the relationship between the principal stresses and the strength envelope also allows the fracturing type to be determined, along with the range of possible orientations with respect to the principal stress directions.

4. Results

4.1. Global fracture pattern from tidal despinning

An assessment of global stresses from tidal despinning (Fig. 3a) shows that three general provinces defined by the relative magni-

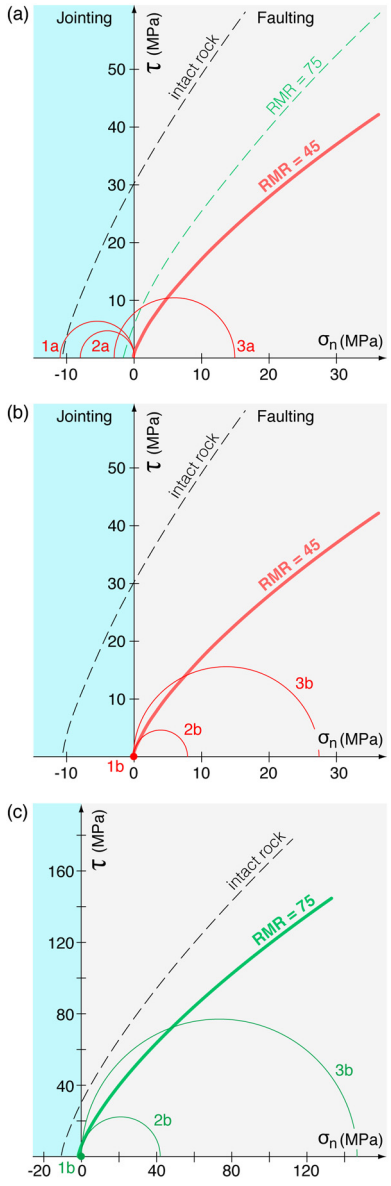

Fig. 4. Mohr diagrams with rock strength envelopes of intact basalt (i.e., an RMR value of 100: black line, dashed), as well as basaltic rock masses with RMR values of 45 and 75 (red and green lines, respectively). Compression is shown as positive. (a) Mohr circles corresponding to stress states from tidal despinning alone for RMR values of 45, shown by latitudinal province (Fig. 3a). All stress states predict tensile fracturing, i.e., opening-mode fractures. (b) Mohr circles for stress states from tidal despinning and global contraction shown by latitudinal province (Fig. 3b) for RMR values of 45. A basaltic rock mass would resist failure at the poles, but thrust faulting is predicted in the equatorial region. (c) Mohr circles for stress states from tidal despinning and global contraction shown for RMR values of 75. The differential stresses are larger than in (b), but as in that case, a basaltic rock mass would be stable at the poles, whereas thrust faulting is predicted in the equatorial region.

tudes of principal stresses must be considered. Principal stresses are evaluated for near-surface conditions, so the overburden stress, which forms the vertical principal stress component, is assumed to equal zero.

Tidal despinning alone produces a latitudinal variation in horizontal principal stresses (Fig. 3a), for which we evaluate the three general provinces defined above. Fig. 4a shows the corresponding Mohr circles for an RMR value of 45. In province 1a (i.e., for latitudes between 90° and 48.5°), the azimuthal and meridional stresses, at nearly equal values, are the greatest tensile stresses, with the overburden the least tensile stress. The Mohr circle for this province plots entirely outside the Mohr strength envelope (thick red line) and exclusively in the tensile regime. The tensile strength of the basaltic rock mass is exceeded and, thus, rock failure should largely be accommodated with mode-I fractures (i.e., joints). Moreover, the intercept of this Mohr circle with the strength envelope specifies the range of orientations at which predicted fractures would form. In this case, since the intercept is at zero, joints of any orientation will form.

In province 2a (i.e., at latitude ±48.5°), the meridional stress component is the most tensile, whereas the azimuthal and overburden stresses are both zero (Fig. 3a). As with province 1a, the resulting Mohr circle plots almost entirely outside the strength envelope and in the tensile regime (Fig. 4a), again predicting the formation of joints. Although joints can still form at any orientation, as the absolute values of meridional stresses are greatest, east–west-oriented jointing is preferred.

For province 3a (i.e., between 48.5°N and 48.5°S), the meridional stress component is tensile, the azimuthal stress component is compressive, and the overburden stress forms the intermediate principal stress component (Fig. 3a). This Mohr circle, too, intersects the strength envelope (Fig. 4a), and so rock failure is predicted. Several combinations of shear and normal stresses can produce failure in both the tensile and compressive regimes. However, the tensile strength of a basaltic rock mass is much lower than its compressive strength, and thus for near-surface stress conditions jointing is likely favored over faulting. Joints would form with a preferred east–west orientation, with deviations from this orientation unlikely to be greater than 40°.

On the basis of Anderson's theory of faulting, previous workers (e.g., Melosh, 1977; Melosh and Dzurisin, 1978; Melosh and McKinnon, 1988) interpreted the relative magnitudes of the stresses (Fig. 3a) to result in normal faults at the poles, strike-slip faults at mid-latitudes, and thrust faults in the equatorial region (Fig. 1). Melosh (1977) recognized that the relationship between stresses and faulting is valid only for a purely compressive stress regime and argued that this condition holds at some depth at which the overburden is sufficient. If the solutions for tidal despinning obtained here for near-surface conditions apply to such depths, and/or if predicted joints grow sufficiently deep, failure by faulting might indeed occur. However, reassessment of stresses within a rock mass shows that the absolute magnitudes of the principal stresses are much lower than for intact rock, and the differential stresses are less as well. With increasing depth, differential stresses stay generally constant whereas principal stresses become more compressive (i.e., the Mohr circles in Fig. 4a would translate along the normal stress axis without an increase in diameter). Basaltic lithospheres are stable for such stress conditions at depths of ~1 km or less and, thus, pervasive surface faulting is unlikely to occur even on a larger scale.

Of course, the driving stresses needed to propagate an existing plane of weakness are much lower than the critical stresses necessary to trigger failure. Joints thus have the potential to serve as planes of weaknesses for later faulting at depth, especially over a narrow range of depths in the polar regions, if they are critically stressed. The majority of joints are not favorably oriented for this condition to be satisfied, however, particularly for fracturing in equatorial regions. Moreover, near-surface conditions there promote vertical, east–west-oriented jointing. Planes of weaknesses so oriented are unlikely to support frictional sliding (Zoback, 2010, p. 132), as the greatest principal stresses are also aligned east–west (Fig. 3a).

Differential stresses for solutions of tidal despinning with an RMR value of 75 are also shown in Fig. 4a. These stresses are greater than, but produce the same results as, the stresses derived for an RMR value of 45.

4.2. Global fracture pattern from tidal despinning and global contraction

Assessments of rock mass stability under the stresses explored for the combination of tidal despinning and global contraction (with a resultant ΔR of 2.9 km) are shown in Fig. 4b (for an RMR value of 45) and Fig. 4c (for an RMR of 75). From both figures, the structural outcomes for provinces 1b, 2b, and 3b may be evaluated. A discussion of the appropriateness of the models, provinces, and scenarios with respect to the timing and duration of the two processes, as well as to the amount of global contraction, is given below.

For an RMR of 45, province 1b does not experience any substantial tectonic stresses, and thus no failure occurs (Fig. 4b, c). Stresses become greater toward lower latitudes, however, with azimuthal stresses increasing at a greater rate. At latitudes of 58° (for an RMR value of 45) or 56° (for an RMR of 75), a critical stress value is reached (province 2b; the Mohr circle intercepts the strength envelope at one point) above which rock failure occurs (Fig. 4b, c). At all lower latitudes (i.e., province 3b), failure in the faulting regime is predicted. As the overburden stresses are zero, the meridional stresses are intermediate, and the azimuthal stress component is the most compressive in this province, thrust faults with north–south orientations are expected to form. The intercept of the Mohr circle with the strength envelope indicates that thrust faults here should form with dip angles no greater than 31° (for an RMR value of 45) to 35° (for an RMR of 75).

5. Discussion

5.1. Tidal despinning versus global contraction: timing and duration

The extent to which a fracture pattern from tidal despinning, with or without global contraction, developed on Mercury can be evaluated only if the timing and duration of these processes are known. The timing and duration of tidal despinning on Mercury, however, are not well constrained. Nonetheless, a number of assumptions regarding its time span can be made. The solutions to Eq. (1) pertain to a scenario under which an early equatorial bulge was fully supported by Mercury's lithosphere. For that condition to hold, a sufficiently thick lithosphere must have been present at the time of initial despinning. The rate and timing of lithospheric thickening depended on the initial thermal state of and early heat flux from the planet's mantle (both of which are poorly constrained), but modeling by Breuer et al. (2007) showed that Mercury's lithosphere could have substantially thickened within ~0.2 Gy of the planet's formation. If stresses from the relaxation of a tidal bulge influenced the formation of a global tectonic fabric for Mercury, then the tidal despinning process either lasted longer than, or initiated after, the first ~0.2 Gy of Mercury's history.

The time span of global contraction can be constrained to first order from observations of the relative timing of activity on thrust faults and the emplacement of volcanic units (Klimczak et al., 2013), or from relations between thrust faults and impact craters (Banks et al., 2014; Ferrari et al., 2015), both of which place the earliest evidence for crustal shortening at ~3.9 Ga. As there is also evidence for geologically recent shortening on Mercury (Klimczak et al., 2013; Banks et al., 2014), it is likely that global contraction operated over much of the last 3.9 Gy and may be ongoing today (Tosi et al., 2013).

Melosh and Dzurisin (1978) presented a tectonic history of Mercury by which much of the relaxation of an equatorial bulge preceded the onset of global contraction and both processes were largely complete by the end of the late heavy bombardment of the inner Solar System. In contrast, Matsuyama and Nimmo (2009) favored a scenario under which tidal despinning, coupled with the reorientation of Mercury caused by the impact that formed the Caloris basin, was a continuous and slow process overlapping with, and potentially outlasting, global contraction.

Whatever the absolute timing of global contraction and tidal despinning, the relative timing and durations of the two processes suggest two end-member scenarios: one in which tidal despinning was followed by global contraction, and another in which both processes temporally overlapped. Both scenarios predict the development of distinct global tectonic fabrics on Mercury, and both have implications for the amount of radius change experienced by the planet. The two scenarios can be evaluated from the global map of tectonic structures (Fig. 2).

5.1.1. Scenario 1: tidal despinning predates global contraction

If tidal despinning occurred after an equatorial bulge was supported by Mercury's lithosphere but before the onset of global contraction, a global fabric of shallow (<1 km) joints would have formed first (Fig. 5a). Such joints would have had no preferred orientations at higher latitudes (i.e., at latitudes poleward of ±48.5°), but structures would have become increasingly east–west-oriented toward the equator. After the relaxation of the equatorial bulge and the formation of the joints, the stresses from tidal despinning would likely have been largely relaxed, so that with the start of global contraction these joints would have probably closed. At the poles, the orientations of the joints were favorable for reactivation by thrust faulting, but joint orientations would have been less susceptible to tectonic reactivation equatorward (see Section 4.1). Therefore, a global thrust fault population developing under these conditions likely formed a planet-wide fabric of randomly oriented structures, with a higher density of faults near the poles.

Under this scenario, stresses from tidal despinning can be assumed to have barely influenced the magnitude and orientation of stresses from global contraction. It follows, then, that the minimum amount of global contraction required to produce the observed faulting is that recorded by observed faults, in addition to the portion of global contraction that Mercury's lithosphere could resist prior to faulting. As shown by Klimczak et al. (2014), Mercury's lithosphere was sufficiently strong to withstand a radius change of 0.29 km (RMR 45) to 1.59 km (RMR 75) prior to the initiation of brittle failure.

5.1.2. Scenario 2: tidal despinning and global contraction temporally overlapped

If tidal despinning and global contraction temporally overlapped, thrust faults initially formed with preferred north–south orientations near the equator (Fig. 5b), as compressive stresses were initially highest there (Fig. 3b). With further increases in compressive stress, thrust faulting propagated poleward, where the near-isotropic horizontal stresses (Fig. 3b) would have resulted in structures with no preferred orientations. A similar thrust fault pattern was described by Melosh and Dzurisin (1978). Since thrust faulting would have initiated near the equator, a higher density of and/or larger dimensions of structures would be expected there.

Under this scenario, the stresses from tidal despinning and global contraction acted on Mercury's lithosphere in concert. The scenario evaluated in Section 4.2 was for a radius decrease of 2.9 km, which did not produce conditions favoring thrust faulting at latitudes poleward of ±58°. However, thrust faults are observed in Mercury's polar regions (Fig. 2a, b). For rock failure to have occurred in Mercury's polar regions under this scenario, a minimum radius decrease of 4.8 km is required. This amount is inclusive of the portion of radius change that the lithosphere can withstand

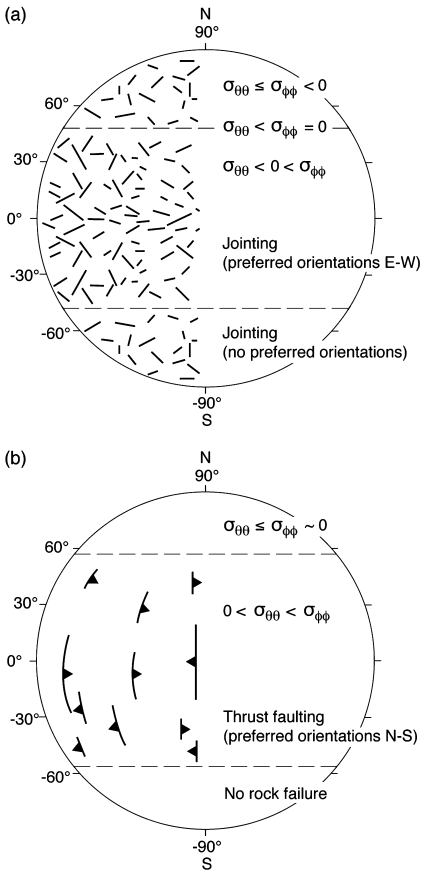

Fig. 5. Schematic depictions of two possible global tectonic patterns for Mercury. (a) Tidal despinning alone would have caused a global set of near-surface joints with no preferred orientations at the poles but with increasingly preferred east–west orientations toward the equator. (b) With combined tidal despinning and global contraction, under a scenario in which Mercury experienced a radius decrease of 2.9 km, stresses were sufficiently large for rock failure to occur only at low and mid-latitudes. There, thrust faults would have preferred north–south orientations.

prior to the onset of thrust faulting (Klimczak et al., 2014) and is consistent with recent estimates from the distribution and dimensions of tectonic structures of the extent to which Mercury has contracted (Byrne et al., 2014) (see below).

5.2. Comparison with observed global pattern

A comprehensive global map of thrust-fault-related landforms on Mercury constructed from MESSENGER orbital observations and shown in Figs. 2a and 2b includes several thousand individual landforms that accommodated horizontal shortening equivalent to 4–7 km of radial contraction (Byrne et al., 2014). To first order, the map does not readily reveal a coherent global pattern of thrust faults. Therefore, the number and orientations of thrust faults were analyzed in latitudinal bins of 30° width (Fig. 2c) (see the Supplemental Material of Byrne et al., 2014). These results indicate that thrust faults between latitudes 60°N and 60°S have preferred north–south orientations. In contrast, those thrust faults at the poles seem not to have preferred orientations. In addition, the spatial density of large thrust faults (i.e., those longer than 50 km) is generally higher at the equator and decreases toward the poles (see the Supplemental Material of Byrne et al., 2014).

The latitudinal variations in thrust fault orientation (Fig. 2c), as well as the amount of cumulative radius change that the full population of thrust faults has accommodated, agree well with predictions from the scenario under which tidal despinning and global contraction temporally overlapped. As discussed by Byrne et al. (2014), however, the maps of tectonic features have observational limitations. The thrust faults were mapped from images acquired by MESSENGER's Mercury Dual Imaging System (MDIS), and those images are strongly influenced by the prevailing illumination conditions at Mercury. As the planet has nearly zero obliquity, solar illumination is from solely the east or the west at low latitudes. Only at high latitudes are landforms subject to a substantially broader range of illumination directions. Such lighting conditions therefore favor the identification of north–south-oriented landforms at equatorial and even mid-latitudes, whereas landforms with a variety of orientations can be recognized in the polar regions.

Furthermore, solar incidence angles of less than ~75° (measured from the zenith) are not optimal for the mapping of landforms that are oriented parallel (i.e., east–west) to the solar illumination azimuth. The high-incidence-angle global base map mosaic of Mercury used in the preparation of the map shown in Fig. 2 still includes large portions of the planetary surface illuminated with incidence angles <75°. The map does not, therefore, include east–west-aligned structures hundreds of kilometers in length, with more than 1000 m of accumulated relief, that have been found in artificially illuminated hillshade maps produced from regional topographic datasets (Preusker et al., 2011). The production of additional topographic models from stereophotogrammetry in the future will complement the mapping of tectonic landforms from MDIS images alone.

6. Conclusions

We have reassessed the magnitude and latitudinal variations of stresses resulting from tidal despinning and the combination of tidal despinning and global contraction, following the method of Melosh and McKinnon (1988), but making use of rock mass rating (RMR) values (Bieniawski, 1989) for the strength properties and deformability of Mercury's lithosphere. This reassessment yields a detailed set of conclusions specific to the tectonic history of Mercury, yet applicable as well to related geophysical problems for other planetary bodies.

An unmodified Young's modulus should be used only when assessing stresses in intact rock (Walsh, 1965; Kulhawy, 1975; Segall, 1984; Kachanov, 1992; Schultz, 1996). Planetary lithospheres are not intact, however, and thus the use of the unmodified Young's modulus for stress calculations on larger scales is inappropriate. In this study, we make use instead of the deformation modulus (Schultz, 1995). Notably, the deformation modulus appropriate for a basaltic rock mass is substantially lower than the respective Young's modulus and thus yields much lower stresses for tidal despinning and global contraction models than previously calculated.

We have compared the revised stresses with the near-surface strength of basaltic rock masses to evaluate the conditions that would lead to rock failure, as well as the fracturing modes and feature orientations that would result. The predicted surface tectonic pattern from tidal despinning alone, contrary to previous findings (e.g., Melosh, 1977), consists of only a global set of opening-mode fractures. The fracture pattern resulting from a combination of tidal despinning and global contraction, on the other hand, consists of a global population of thrust faults, similar to that presented by Melosh and Dzurisin (1978).

Under the assumptions that tidal despinning and global contraction both operated on Mercury at some point in its past, and that an equatorial bulge was supported by the planet's lithosphere, we then assess two end-member scenarios: (1) where tidal despinning predated global contraction, and (2) where tidal despinning

and global contraction temporally overlapped. Both scenarios yield specific, testable results:

(1) If tidal despinning predated global contraction, Mercury should possess a global thrust fault population with no preferred structural orientations. Under this scenario, more thrust faults should have formed at the poles than at mid- to low latitudes, and the lower limit on the amount of global contraction should be essentially that measured from mapped thrust faults alone (Byrne et al., 2014).
(2) If tidal despinning and global contraction temporally overlapped, Mercury's global tectonic fabric should feature a population of thrust faults with north–south orientations at the equator and mid latitudes and thrust faults with no preferred orientations at the poles. Under this scenario, more thrust faults should have formed in the equatorial region, and the amount of radius change from global contraction must have been greater than 4.8 km to satisfy the observation that thrust faults are found in the polar regions.

Despite the effect of a lighting bias on the current global map of tectonic features, there is a broad agreement between MESSENGER observations and the predicted latitudinal variations in orientation of thrust faults, as well as between the predicted minimum amount of radius change and the radius change calculated from the mapping results, under the latter scenario. Mercury's global fabric of thrust faults may therefore record a global tectonic environment in which stresses from tidal despinning and global contraction both played roles.

Acknowledgements

We thank Michelle Selvans and Thomas Watters for helpful discussion, and we thank Christophe Sotin and an anonymous reviewer for constructive comments on an earlier draft. The MESSENGER project is supported by the NASA Discovery Program under contracts NASW-00002 to the Carnegie Institution of Washington and NAS5-97271 to The Johns Hopkins University Applied Physics Laboratory.

References

Banks, M.E., Klimczak, C., Xiao, Z., Watters, T.R., Strom, R.G., Braden, S.E., Chapman, C.R., Solomon, S.C., Byrne, P.K., 2014. Duration of activity on lobate-scarp thrust faults on Mercury. Lunar Planet. Sci. 45, abstract 2722.
Beuthe, M., 2010. East–west faults due to planetary contraction. Icarus 209, 795–817.
Bieniawski, Z.T., 1989. Engineering Rock Mass Classifications. Wiley, New York.
Breuer, D., Hauck II, S.A., Buske, M., Pauer, M., Spohn, T., 2007. Interior evolution of Mercury. Space Sci. Rev. 132, 229–260.
Burns, J.A., 1975. The angular momenta of solar system bodies: implications for asteroid strengths. Icarus 25, 545–554.
Burns, J.A., 1976. Consequences of the tidal slowing of Mercury. Icarus 28, 453–458.
Byrne, P.K., Klimczak, C., Şengör, A.M.C., Solomon, S.C., Watters, T.R., Hauck II, S.A., 2014. Mercury's global contraction much greater than earlier estimates. Nat. Geosci. 7, 301–307.
Di Achille, G., Popa, C., Massironi, M., Epifani, E.M., Zusi, M., Cremonese, G., Palumbo, P., 2012. Mercury's radius change estimates revisited using MESSENGER data. Icarus 221, 456–460.
Dombard, A.J., Hauck II, S.A., 2008. Despinning plus global contraction and the orientation of lobate scarps on Mercury: predictions for MESSENGER. Icarus 198, 274–276.
Fassett, C.I., Head, J.W., Baker, D.M.H., Zuber, M.T., Smith, D.E., Neumann, G.A., Solomon, S.C., Klimczak, C., Strom, R.G., Chapman, C.R., Prockter, L.M., Phillips, R.J., Oberst, J., Preusker, F., 2012. Large impact basins on Mercury: global distribution, characteristics, and modification history from MESSENGER orbital data. J. Geophys. Res. 117, E00L08. http://dx.doi.org/10.1029/2012JE004154.
Ferrari, S., Massironi, M., Marchi, S., Byrne, P.K., Klimczak, C., Martellato, E., Cremonese, G., 2015. Age relations of Rembrandt basin and Enterprise Rupes, Mercury. In: Platz, T., Massironi, M., Byrne, P.K., Hiesinger, H. (Eds.), Volcanism and Tectonism across the Inner Solar System. In: Geol. Soc. London Spec. Pub., vol. 401, pp. 159–172.
Galluzzi, V., Di Achille, G., Ferranti, L., Popa, C., Palumbo, P., 2015. Faulted craters as indicators for thrust motions on Mercury. In: Platz, T., Massironi, M., Byrne, P.K., Hiesinger, H. (Eds.), Volcanism and Tectonism across the Inner Solar System. In: Geol. Soc. London Spec. Pub., vol. 401, pp. 313–325.
Hoek, E., Brown, E.T., 1980. Empirical strength criterion for rock masses. J. Geotech. Eng. Div. Am. Soc. Civil Eng. 106, 1013–1035.
Kachanov, M., 1992. Effective elastic properties of cracked solids: critical review of some basic concepts. Appl. Mech. Rev. 45, 304–335.
Kaula, W., 1968. Introduction to Planetary Physics: The Terrestrial Planets. Wiley, New York.
Klimczak, C., Byrne, P.K., Banks, M.E., Solomon, S.C., Fassett, S.C., Ostrach, L.R., Ferrari, S., Denevi, B.W., Ernst, C.M., Preusker, F., 2013. The relative timing of global contraction and plains volcanism on Mercury. Geological Society of America Abstracts with Programs 45, 295.
Klimczak, C., Byrne, P.K., Solomon, S.C., 2014. Limits on the strength of lithospheres undergoing global contraction. Lunar Planet. Sci. 45, abstract 1542.
Kulhawy, F.H., 1975. Stress deformation properties of rock and rock discontinuities. Eng. Geol. 9, 327–350.
Massironi, M., Di Achille, G., Rothery, D., Galluzzi, V., Giacomini, L., Ferrari, S., Zusi, M., Cremonese, G., Palumbo, P., 2015. Lateral ramps and strike-slip kinematics on Mercury. In: Platz, T., Massironi, M., Byrne, P.K., Hiesinger, H. (Eds.), Volcanism and Tectonism across the Inner Solar System. In: Geol. Soc. London Spec. Pub., vol. 401, pp. 269–290.
Matsuyama, I., Nimmo, F., 2009. Gravity and tectonic patterns of Mercury: effect of tidal deformation, spin–orbit resonance, nonzero eccentricity, despinning, and reorientation. J. Geophys. Res. 114, E01010. http://dx.doi.org/10.1029/2008JE003252.
Melosh, H.J., 1977. Global tectonics of a despun planet. Icarus 31, 221–243.
Melosh, H.J., Dzurisin, D., 1978. Mercurian global tectonics: a consequence of tidal despinning? Icarus 35, 227–236.
Melosh, H.J., McKinnon, W.B., 1988. The tectonics of Mercury. In: Vilas, F., Chapman, C.R., Matthews, M.S. (Eds.), Mercury. University of Arizona Press, Tucson, Ariz., pp. 374–400.
Nahm, A.L., Schultz, R.A., 2007. Outcrop-scale physical properties of Burns Formation at Meridiani Planum, Mars. Geophys. Res. Lett. 34, L20203. http://dx.doi.org/10.1029/2007GL031005.
Nittler, L.R., Starr, R.D., Weider, S.Z., McCoy, T.J., Boynton, W.V., Ebel, D.S., Ernst, C.M., Evans, L.G., Goldsten, J.O., Hamara, D.K., Lawrence, D.J., McNutt Jr., R.L., Schlemm, C.E., Solomon, S.C., Sprague, A.L., 2011. The major-element composition of Mercury's surface from MESSENGER X-ray spectrometry. Science 333, 1847–1850.
Pechmann, J.B., Melosh, H.J., 1979. Global fracture patterns of a despun planet: application to Mercury. Icarus 38, 243–250.
Preusker, F., Oberst, J., Head, J.W., Watters, T.R., Robinson, M.S., Zuber, M.T., Solomon, S.C., 2011. Stereo topographic models of Mercury after three MESSENGER flybys. Planet. Space Sci. 59, 1910–1917.
Schultz, R.A., 1993. Brittle strength of basaltic rock masses with applications to Venus. J. Geophys. Res. 98, 10883–10895.
Schultz, R.A., 1995. Limits on strength and deformation properties of jointed basaltic rock masses. Rock Mech. Rock Eng. 28, 1–15.
Schultz, R.A., 1996. Relative scale and the strength and deformability of rock masses. J. Struct. Geol. 18, 1139–1149.
Schultz, R.A., Okubo, C.H., Wilkins, S., 2006. Displacement–length scaling relations for faults on the terrestrial planets. J. Struct. Geol. 28, 2182–2193.
Segall, P., 1984. Formation and growth of extensional fracture sets. Geol. Soc. Am. Bull. 95, 454–462.
Solomon, S.C., 1977. The relationship between crustal tectonics and internal evolution on the Moon and Mercury. Phys. Earth Planet. Inter. 15, 135–145.
Strom, R.G., Trask, N.J., Guest, J.E., 1975. Tectonism and volcanism on Mercury. J. Geophys. Res. 80, 2478–2507.
Tosi, N., Grott, M., Plesa, A.-C., Breuer, D., 2013. Thermochemical evolution of Mercury's interior. J. Geophys. Res. Planets 118, 2474–2487.
Vening-Meinesz, F.A., 1947. Shear patterns on the Earth's crust. Trans. Am. Geophys. Union 28, 1–61.
Walsh, J.B., 1965. The effect of cracks on the uniaxial compression of rocks. J. Geophys. Res. 70, 399–411.
Watters, T.R., Nimmo, F., 2010. The tectonics of Mercury. In: Watters, T.R., Schultz, R.A. (Eds.), Planetary Tectonics. Cambridge University Press, Cambridge, pp. 15–80.
Watters, T.R., Robinson, M.S., Cook, A.C., 1998. Topography of lobate scarps on Mercury: new constraints on the planet's contraction. Geology 26, 991–994.
Watters, T.R., Solomon, S.C., Robinson, M.S., Head, J.W., André, S.L., Hauck II, S.A., Murchie, S.L., 2009. The tectonics of Mercury: the view after MESSENGER's first flyby. Earth Planet. Sci. Lett. 285, 283–296.
Wieczorek, M.A., Neumann, G.A., Nimmo, F., Kiefer, W.S., Taylor, G.J., Melosh, H.J., Phillips, R.J., Solomon, S.C., Andrews-Hanna, J.C., Asmar, S.W., Konopliv, A.S., Lemoine, F.G., Smith, D.E., Watkins, M.M., Williams, J.G., Zuber, M.T., 2013. The crust of the Moon as seen by GRAIL. Science 339, 671–675. http://dx.doi.org/10.1126/science.1231530.
Weider, S.Z., Nittler, L.R., Starr, R.D., McCoy, T.J., Stockstill-Cahill, K.R., Byrne, P.K., Denevi, B.W., Head, J.W., Solomon, S.C., 2012. Chemical heterogeneity on

Mercury's surface revealed by the MESSENGER X-Ray Spectrometer. J. Geophys. Res. 117, E00L05. http://dx.doi.org/10.1029/2012JE004153.

Zoback, M.D., 2010. Reservoir Geomechanics. Cambridge University Press, Cambridge.

Zuber, M.T., Smith, D.E., Lehman, D.H., Hoffman, T.L., Asmar, S.W., Watkins, M.M., 2013. Gravity Recovery and Interior Laboratory (GRAIL): mapping the lunar interior from crust to core. Space Sci. Rev. 178, 3–24. http://dx.doi.org/10.1007/s11214-012-9952-7.